

# Atomistic simulations of a multicomponent asymmetric lipid bilayer

Anirban Polley<sup>1</sup>, Satyavani Vemparala<sup>2</sup>, and Madan Rao<sup>1,3\*</sup>

<sup>1</sup>*Raman Research Institute, C.V. Raman Avenue, Bangalore 560080, India*

<sup>2</sup>*The Institute of Mathematical Sciences, CIT Campus, Chennai 600 113, India*

<sup>3</sup>*National Centre for Biological Sciences (TIFR), Bellary Road, Bangalore 560065, India*

E-mail: madan@rri.res.in

## Abstract

The cell membrane is inherently asymmetric and heterogeneous in its composition, a feature that is crucial for its function. Using atomistic molecular dynamics simulations, the physical properties of a 3-component asymmetric mixed lipid bilayer system comprising of an unsaturated POPC (palmitoyl-oleoyl-phosphatidyl-choline), a saturated SM (sphingomyelin) and cholesterol are investigated. In these simulations, the initial stages of liquid ordered,  $l_o$ , domain formation are observed and such domains are found to be highly enriched in cholesterol and SM. The current simulations also suggest that the cholesterol molecules may partition into these SM-dominated regions in the ratio of 3 : 1 when compared to POPC-dominated regions. SM molecules exhibit a measurable tilt and long range tilt correlations are observed within the  $l_o$  domain as a consequence of the asymmetry of the bilayer, with implications to local membrane deformation and budding. Tagged particle diffusion for SM and cholesterol molecules, which reflects spatial variations in the physical environment encountered by the tagged particle, is computed and compared with recent experimental results obtained from high resolution microscopy.

---

\*To whom correspondence should be addressed

## Introduction

The cell membrane is characterized by both lateral and transverse lipid heterogeneity, an aspect of significant functional consequence.<sup>1</sup> Transverse lipid heterogeneity is maintained actively by the cell, making the cell bilayer intrinsically asymmetric. Lateral lipid heterogeneities called ‘rafts’,<sup>2,3</sup> which are ternary mixtures of sphingomyelin (SM), phosphatidyl Choline (PC) and cholesterol (Chol) molecules have been implicated in a variety of cellular processes including signaling and endocytosis, even though the nature of these functional cellular rafts is still a matter of contention.<sup>4-7</sup> Asymmetry in bilayers can arise both in terms of difference in constituent lipids or in number of lipid molecules in both leaflets. In spite of this obvious lateral/transverse compositional heterogeneity, except for a few seminal studies,<sup>8</sup> most in-vitro investigations of multicomponent artificial membranes<sup>9-11</sup> have been done on symmetric bilayers. Further, most of the atomistic simulations of model cell membrane mimics, have been carried out on systems which either have lateral heterogeneity<sup>12</sup> or transverse asymmetry<sup>13-15</sup> but rarely both. There have however been a few studies using coarse-grained simulations<sup>16,17</sup> and continuum Landau theories<sup>18-20</sup> that address the role of inter-bilayer coupling in equilibrium physical properties and domain growth.

While early simulations of model membranes consisted only of a single-component PC bilayers,<sup>21-23</sup> later simulations have incorporated more than one lipid component, in particular cholesterol.<sup>24</sup> Following the ‘raft proposal’ of the importance of SM molecules in raft formation, an increasing number of simulations with SM molecules<sup>25</sup> have been carried out. These simulations include detailed comparisons between mixtures of SM and Chol and PC and Chol.<sup>12,26-30</sup> Finally, simulations on asymmetric bilayers have also been reported. A simulation study by Bhide et al.<sup>31</sup> was performed on systems consisting of SM and Chol molecules in upper leaflet and SOPS and Chol molecules in the lower leaflet, with equal number of phospholipids in both the leaflets. Comparisons between each leaflet of the asymmetric bilayer with corresponding simulations of symmetric bilayers showed no significant differences in their physical properties.

In this paper, the equilibrium properties of a multicomponent asymmetric (both lateral and transverse) bilayer using atomistic molecular dynamics (MD) simulations are studied. Specifically,

the physical properties of a 3-component asymmetric lipid bilayer comprising of an unsaturated POPC, a saturated SM and Chol molecules, which exhibits lateral compositional heterogeneities in the form of liquid ordered ( $l_o$ ) - liquid disordered ( $l_d$ ) domains, thought to represent the characteristic lipid composition of rafts on the cell membrane. In addition to studying a variety of order parameters, their correlations and spatial distribution, transport properties of the component lipid molecules are also studied. This study suggests that the presence of lateral heterogeneities in the bilayer can potentially affect the molecular diffusion at short time scales, which may be of relevance to molecular diffusion at the cell surface. However lipid based lateral heterogeneities on the cell surface are likely to be small and below optical resolution; it is only recently that advances in high resolution single-particle tracking (SPT)<sup>32,33</sup> allow one to measure subtle changes in diffusion characteristics as molecules move across the heterogeneous cell surface. In addition, the transverse asymmetry would suggest that the diffusion characteristics of the molecule is different in the two leaflets of the bilayer. Correlations between the local physical environment and the tagged particle diffusion are also investigated in this paper.

## Materials and Methods

Two bilayer model systems have been simulated : (A) a symmetric three-component bilayer consisting of 170 POPC, 171 palmitoyl-sphingomyelin (SM, saturated lipid) and 171 Chol (ratio of 1 : 1 : 1) in each leaflet and (B) an asymmetric bilayer with a composition of 170 POPC, 168 SM and 171 Chol (ratio of roughly 1 : 1 : 1) in the upper leaflet and 256 POPC and 256 Chol (ratio 1 : 1) in the lower leaflet. Two control systems have also been simulated, which are (C) a symmetric one-component bilayer made up of 128 pure POPC and (D) a symmetric two-component bilayer made up of 64 POPC and 64 Chol (ratio 1 : 1 in both leaflets).

The force field parameters for POPC were taken from the previously validated united-atom description (Tielman and Berendsen<sup>34</sup>), whereas for SM and Chol, parameters from works of Niemela et al.<sup>12</sup> were used. Water was simulated by the simple point charge (SPC) model<sup>35</sup> and

PACKMOL<sup>36</sup> was used to generate the initial configurations of all the bilayer systems and hydrated with water in the ratio of 1(lipid) : 32 (water).

All MD simulations were performed at a temperature  $T = 296\text{K}$ , which lies between the main transition temperatures of POPC ( $T_m = -2.9 \pm 1.3^\circ\text{C}$ )<sup>37</sup> and SM ( $T_m \approx 41.4^\circ\text{C}$ )<sup>38</sup> and right in the middle of the  $l_o$ - $l_d$  phase coexistence region of the symmetric ternary system.<sup>39</sup> GROMACS (<http://www.gromacs.org>)<sup>40</sup> software was used to integrate the equations of motion with a time step of 2 fs. To avoid bad contacts arising from steric constraints during initialization, all bilayer systems were subjected to steepest descent minimization initially. The systems were then simulated for 50 ps in the NVT ensemble using a Langevin thermostat. Subsequently, each system was simulated in the NPT ensemble ( $T = 296\text{K}$ ,  $P = 1\text{atm}$ ) using a Berendsen thermostat and semi-isotropic pressure coupling with compressibility  $4.5 \times 10^{-5} \text{ bar}^{-1}$  for 220 ns (for the asymmetric ternary system *B*) and for 100 ns (for symmetric ternary system *A*) and for 100 ns (for the single and two -component systems *C* and *D*). Lipid system parameters such as deuterium order parameter and mean thickness were monitored throughout the simulations to ensure that the system is well equilibrated. All the reported results are computed over last 20ns unless otherwise stated.

Note that the two model systems *A* and *B* have been simulated starting from two sets of initial conditions : (i) where the components in each leaflet are mixed or (ii) where the ternary components are completely phase segregated.

## Results

To make sure that a stable, surface tension-less asymmetric bilayer is being simulated, the forces, torques and surface tension of the bilayer are computed from the local stress tensor  $\sigma_{ij}(x, y, z) = \frac{1}{v} \sum_{\alpha} f_i^{\alpha} r_j^{\alpha}$ , where  $f_i^{\alpha}$  is the  $i^{\text{th}}$  component of the force on the  $\alpha^{\text{th}}$ -particle due to all other particles within a coarse-grained volume  $v = [0.1 \text{ nm}]^3$ . The net force  $F_i = \int \partial_k \sigma_{ik} dv$  and its first moment (related to the torque)  $M_{ik} = \int (\partial_l \sigma_{il} x_k - \partial_l \sigma_{kl} x_i) dv$  for the bilayer were computed and both force and torque balance  $-F_1 = 0.29 \pm 3.34$ ,  $F_2 = -2.56 \pm 2.09$ ,  $F_3 = -2.16 \pm 3.2$ , in units of nN and

$M_{12} = 0.77 \pm 0.428, M_{13} = -8.83 \pm 2.04, M_{23} = -13.303 \pm 1.67$ , in units of nN·nm were achieved suggesting a mechanically stable asymmetric bilayer. These are comparable to the corresponding values for the symmetric bilayers (see Supplementary Information). The membrane surface tension is calculated as  $\gamma = \int \pi(z) dz$ , integrated over the width of the bilayer, where  $\pi(z)$  is the lateral pressure, given by  $\pi(z) = \frac{1}{2} (\bar{\sigma}_{xx}(z) + \bar{\sigma}_{yy}(z)) - \bar{\sigma}_{zz}(z)$ ,<sup>41,42</sup> resulting in a value of  $\gamma = -0.0018 \pm 0.0301$  bar·nm, essentially a ‘zero’ surface tension bilayer. More details of time dependence of net forces, their moments and surface tension are provided in Supplementary Figure S2. A snapshot of the equilibrium bilayer configuration of the asymmetric membrane is shown in Figure 1(a). In Figure 1(b), the pressure profiles of symmetric and asymmetric bilayers are shown for comparison. In contrast to the asymmetric bilayer, the symmetric bilayer exhibits a symmetric pressure profile about the midplane. On the other hand the pressure profile of the asymmetric bilayer shows larger spatial oscillations.

## Lipid composition

At the temperature and overall lipid composition under consideration, the homogeneous mixed phase of both the asymmetric and symmetric bilayers is unstable and exhibits definite features of phase separation between POPC-rich and SM-rich domains (Supplementary Figures, S3, S4); in the asymmetric bilayer phase segregation occurs in the upper leaflet alone, while the composition in the lower leaflet remains homogeneous. To show that the bilayer is undergoing phase separation towards a final equilibrium phase segregated configuration, the theory of dynamical coarsening,<sup>43</sup> which deals with the study of the dynamics of domain formation starting from a complete disordered phase is used. In simulations starting from an initial mixed state, it was found that the system quickly phase segregates; at early times the domain sizes are small and grow over the simulation time, 220 ns. It has been shown earlier that complete phase segregation occurs only over a very long time, at least on a microsecond time scale.<sup>44,45</sup> To demonstrate dynamics of domain formation or coarsening, we have computed (i) the probability distribution  $P(\phi)$  of the order parameter  $\phi = \frac{\rho_{SM} - \rho_{POPC}}{\rho_{SM} + \rho_{POPC}}$  at different times (where  $\rho_{SM/POPC}$  is the local density of SM/POPC), and (ii) the

energy density  $\varepsilon = E/V$ , where the energy  $E \propto \int d^2r (\nabla\phi)^2$ , which measures the time dependence of the amount of interface separating the two phases. The results are shown in Figure 2. Initially  $P(\phi)$  is peaked at  $\phi = 0$  (mixed state) and subsequently evolves into a distribution with two peaks at  $\pm 1$  which gets progressively sharper with time. Dynamical scaling in the coarsening regime<sup>43</sup> implies that  $\varepsilon \sim t^{-1/z}$ , where  $z = 3$ , since the order parameter is conserved. Our simulations show that  $1/z = 0.30 \pm 0.15$ , consistent with this scaling prediction (Figure 2 (a)).

The domains are observed to be larger in the symmetric bilayers compared to the asymmetric bilayer, when measured over the total simulation time scale (220 ns). The interfacial fluctuations of the  $l_o$ -domains in the asymmetric bilayer are larger than the symmetric bilayer, suggesting, in line with earlier simulations,<sup>45</sup> that the interfacial tension between the domains is higher in the symmetric bilayer. Both the larger interfacial tension and the enhanced correlations between the domains in the two leaflets of the symmetric bilayer (seen in Supplementary Figure, S4), are a result of a transbilayer coupling. This transbilayer correlation between domains can be understood within a Landau description of both equilibrium and dynamics, in which the relative concentration of lipids in one leaflet acts as a “field” for the concentration in the other leaflet.<sup>20</sup> Local equilibrium relates the domain growth velocity to the interfacial tension,<sup>43</sup> this suggests that the domains coarsen faster in the symmetric bilayer, consistent with our simulations.

To estimate the relative partitioning of cholesterol in the POPC and the SM rich regions in the upper leaflet, the joint probability distribution of finding a given concentration of SM with Chol in an  $xy$  region (similarly, POPC with Chol) is calculated and shown in Figure 2 (b) and 2 (c). These joint probabilities show that the cholesterol concentration completely correlates with the SM concentration (i.e., Chol is low (high) when the SM concentration is low (high)) and completely *anticorrelates* with the POPC concentration (i.e., Chol is low (high) when POPC is high (low)). The joint probability densities plotted in Figures 2(b) and (c) strongly suggest that cholesterol preferentially partitions in the SM-rich phase three times more than in POPC-rich region (more precisely 2.97 : 1)

The segregation of chemical composition is accompanied by changes in physical characteristics

of the segregated molecules. The saturated lipid tails of SM that are in the SM-enriched domains are found to be more rigid than both the SM and POPC molecules in the POPC-rich domains. The deuterium order parameter ( $S$ ) describing the rigidity of lipid tails is computed for SM molecules in both the leaflets and is shown in Figure 4. The probability distribution,  $P(S)$ , of SM gives indication of the location of SM in either SM-rich (higher value) or POPC-rich domains (lower value). As seen in Figure 3(a),  $P(S)$  has a bimodal distribution. The distinction of the deuterium order parameter in the two regions indicate that the SM- and POPC-rich regions may be identified with  $l_o$ -like and  $l_d$ -like phases, respectively. From Figure 3(a), it can be seen that the probability distribution of deuterium order parameters in the asymmetric bilayers are comparable to that of symmetric bilayer. The spatial variation of the deuterium order parameter in the  $x-y$  plane for both asymmetric and symmetric bilayers is shown in Supplementary Figure S7 and it can be noted that the segregation of chemical composition is naturally accompanied by an  $l_o$ - $l_d$ -like phase separation in the bilayer membrane. From this spatial distribution, it can be seen that the size of  $l_o$ -like domain size (enriched in SM) is significantly larger in the symmetric bilayer compared to that of asymmetric bilayer, over the time scale measured.

The probability distribution and the spatial profile of the local bilayer thickness is also computed and shown in Figure 3(b) and Supplementary Figure S7 respectively. The SM-enriched  $l_o$ -like domains have a larger bilayer thickness compared to the POPC-enriched  $l_d$ -like domains. As with deuterium order parameter, the distribution of bilayer thickness for both the symmetric and asymmetric bilayers is bimodal, corresponding to the  $l_d$ -like and  $l_o$ -like domains. It is significant that the difference in the bilayer thickness between the  $l_o$ -like and  $l_d$ -like phases in the symmetric bilayer is consistent with recent AFM studies,<sup>46</sup> and is *more than twice compared to asymmetric bilayer*. The spatial profile of the thickness shown in Supplementary Figure S7 is an accurate measure of the domain size and consistent with the deuterium order parameter results, the domain size in the symmetric bilayer is larger than that of asymmetric bilayer over the time scale measured.

By computing the joint probability of finding SM molecules in the upper and lower leaflets of the symmetric bilayer, it can be seen (Supplementary Figure S5) that there is a clear registry of

SM-rich ( $l_o$ -like) domains across the leaflets, which may be responsible for observed increase in SM-rich domain sizes in symmetric bilayers.

## Lipid splay and tilt

To quantify the relative packing of lipid chains, the amount of splay between the two lipid tails is calculated, in addition to deuterium order parameter computed above. A tail vector is defined as a vector originating from the carbon of the carbonyl group and pointing to the terminal methyl carbon of a lipid tail. The splay angle is the angle between two such tail vectors of each lipid. Simulation results suggest that the extent of splay in SM lipid tails is significantly smaller in  $l_o$ -like domain ( $17^\circ$ ) compared to POPC-rich domain ( $40^\circ$ ) as seen in Supplementary Figure S6. In addition, the extent of lipid splay in the symmetric and asymmetric bilayers is comparable. The spatial heterogeneity of the splay in the asymmetric bilayer reflects the differences in lipid composition (Supplementary Figure, S8). Taken together with the deuterium order parameter data, the lipid splay results strongly suggest that the packing fraction of lipids in the SM-rich phase is higher than that in the POPC-rich phase.

Tilt angle of the lipid tail chain is defined as the orientation of the mean tail vector of the lipid with respect to the local outward normal to the membrane, and is described by two angles ( $\theta, \phi$ ), the polar and azimuthal angles, respectively. The angle  $\phi$  measures the orientation of the 2d tilt vector, the projection of the tail vector onto the tangent plane, with the  $x$ -axis. An accurate determination of the tilt angles of the component lipids is quite involved, since, over short length scales, the local normal to the membrane fluctuates due to molecular protrusion effects. To compute local average tilt, a coarse-graining scale is chosen, which should be more than the protrusion scale and less than the tilt correlation length (which in turn should of course be smaller than the size of the  $l_o$ -like domain). Over this coarse-grained scale, a membrane normal is considered to be along the  $z$ -axis. A convenient choice of coarse graining scale is around a  $1 \text{ nm}^2$  (which encompasses  $\approx 3$  lipids on an average), for which statistically reliable results can be obtained. For instance, for POPC-only bilayer, the probability distribution of the coarse-grained angle,  $P(\theta)$ , is peaked about



zero, while the distribution  $P(\phi)$  is uniform, consistent with the known fact that POPC does not exhibit a tilt at this temperature.

Following such a procedure for computing local tilt angles for the ternary membrane is problematic, since over the timescale of the MD simulation, the size of the  $l_o$ -like domains are small, making it difficult to obtain an unambiguous determination of tilt and its correlations. To address this issue, simulation of a ternary bilayer starting from a completely phase segregated configuration with cholesterol distributed, between SM-rich and POPC-rich domains, in the ratio of 3:1 (as described in Materials and Methods) is carried out. In this case the  $l_o$ -like domain (SM-rich) size is around half the system size and can provide good statistics.

The tilt angle distribution of POPC lipids in the symmetric and asymmetric ternary bilayers has a similar distribution as in the case of POPC-only bilayer as seen in Supplementary Figure S9. On the other hand, the tilt angle distribution for SM shows an interesting trend. While SM in the symmetric bilayer shows no evidence of tilt ( $P(\theta)$  is peaked at around  $0^\circ$  and  $P(\phi)$  is uniform), SM in the SM-rich ( $l_o$ -like) domain of the asymmetric bilayer has a nonzero tilt of around  $2.016 \pm 0.69^\circ$ . This small tilt of SM in the asymmetric bilayer is consistent with the decrease in bilayer thickness of the asymmetric membrane compared to that of symmetric bilayer (see Figure 3(b)). Tilt angle correlations defined as  $C(r) = \langle \phi(r)\phi(0) \rangle$  are computed for POPC and SM lipid molecules and the results are shown in Figure 4. The correlation functions of the tilt of POPC and SM (symmetric bilayer) decay exponentially to zero, consistent with the above findings. However,  $C(r)$  for SM in the asymmetric bilayer decays exponentially to a non zero value, signaling long range order<sup>47</sup> in SM molecules in the asymmetric bilayer. This suggests that the asymmetric nature of the bilayer can potentially generate a tilt ordering of SM molecules in the SM-rich ( $l_o$ -like) domain.

Previous simulations<sup>12,45,48</sup> and experiments<sup>9,49–53</sup> have shown that the thickness of  $l_o$  domains is larger than that of  $l_d$  domain. This difference in thickness between  $l_o$  and  $l_d$  domains gives rise to line tension along the domain boundary.<sup>51</sup> The lipid tails of the  $l_o$  domain can be exposed to solvent as a result of such mismatch, which is energetically unfavourable. One of the ways to

mitigate such mismatch is for the thicker  $l_o$  domain to undergo a small tilt such that the head groups of the two domains can be at the same height. The observed small tilt in the simulations of asymmetric bilayers supports this hypothesis. Within a Landau theory, the asymmetric bilayer can be thought of as being subjected to a transverse compression, which would naturally lead to a tilt when the lipids are stretched out (as they are in the  $l_o$  domain).<sup>54,55</sup>

The existence of a finite tilt and its correlation over long scales, if verified experimentally,<sup>56</sup> could have important consequences for membrane deformation and budding.<sup>57</sup> The tilt vector naturally couples to the local curvature tensor of the membrane, giving rise to anisotropic bending stresses. If the constituent molecules are chiral (as they usually are), then there are additional bending stresses coming from chiral couplings of the tilt and curvature. If strong enough, these bending stresses can induce membrane deformation giving rise to spherical buds or cylindrical tubules.<sup>51,57</sup>

## Tagged particle diffusion

Even though the membrane composition forms stable domains at equilibrium, the individual component molecules can traverse across domains. The equilibrium dynamics of certain ‘tagged’ component lipids can be monitored by measuring their diffusion coefficients and correlating them with the physical and chemical heterogeneity across the membrane. The mean square displacement (MSD) is defined as  $\langle \delta r_i(t)^2 \rangle$  of a tagged particle, where  $\delta r_i(t) = r_i(t) - r_i(0)$  is the displacement of tagged  $i^{th}$  lipid of a given species at time  $t$  from its position at  $t = 0$ . While computing the MSD, the location of the tagged lipid, whether it is in the POPC-rich ( $l_d$ -like) or SM-rich ( $l_o$ -like) domain, is monitored by computing the instantaneous deuterium order parameter  $S$  of the tagged lipid and the local bilayer thickness. The diffusion analysis is show in Figure 5. It can be seen that the diffusion coefficient of both SM and Chol molecules, given by the saturation value of  $\langle \delta r_i^2(t) \rangle / 4t$ , is different depending on whether the tagged lipid molecule is in the  $l_o$ -like and  $l_d$ -like domain as has been reported in other simulation studies.<sup>45</sup>

For tagged SM or Chol molecules that initially lie in the POPC-rich ( $l_d$ -like) domain, the local

diffusion coefficient crosses over from an early time high value ( $D_0$ ) to a late time low value ( $D_\infty$ ). For each of the tagged components, a first-passage time, defined as the first time that a tagged molecule residing in a domain moves out of it, is computed. The crossover time  $\tau$  is then obtained from such a computed first-passage time. The MSD is found to obey a crossover scaling relation,

$$\langle \delta r^2 \rangle = 4D_0 t F(t/\tau) \quad (1)$$

where the nonlinear scaling function  $F$  has the asymptotic form,

$$\begin{aligned} F(t/\tau) &= 1 && \text{for } t/\tau \ll 1 \\ &= \frac{D_\infty}{D_0} && \text{for } t/\tau \gg 1 \end{aligned} \quad (2)$$

The data collapse shown in Figures 5(a) and 5(b) demonstrate this crossover scaling for SM and Chol molecules, respectively. Experimentally the crossover time scale  $\tau$  can be obtained from the value of  $t$  at which the instantaneous  $D(t) = (D_0 + D_\infty)/2$ , rather than the first-passage time. The values of the diffusion coefficients for SM molecules (Fig. 5(a)) are in agreement with the experimental findings,<sup>58,59</sup> while the values for Chol molecules (Fig. 5(b)) are slightly lower than those reported in other simulations.<sup>45</sup> This discrepancy can be attributed to the differences in lipid composition of the ternary bilayer used in both the simulations. The difference in the tagged particle diffusion coefficient between the two domains can be attributed to changes in local viscosity ( $\eta$ ), moment-of-inertia ( $I$ ) of the particle and to changes in the local density correlations (given by the local partial structure factors,  $S_{\alpha\beta}(q)$ ) with neighbouring molecules that the tagged particle experiences as it traverses across the domain. The change in the deuterium order parameter  $S$  is used to track the changes in moment-of-inertia of the tagged molecules. For SM molecules, this shows a crossover similar to the crossover diffusion, with the value of  $S$  being low (high) when the diffusion coefficient is high (low) as seen in Figure 5(a). On the other hand cholesterol being a rigid molecule is unlikely to undergo any conformational change, resulting change in moment-of-inertia, as it traverses across the domains. Thus a substantial change in the diffusion coefficient of

Chol molecules can be attributed to the changes in viscosity and local density correlations,  $S_{\alpha\beta}(q)$ , arising from changes in the local environment.

In the context of SPT experiments, if the time scale over which the tagged particle is tracked is large enough so that the particle crosses and recrosses the domains, then one would measure the MSD of  $\delta r_i(t) = \int dt' (r_i(t'+t) - r_i(t'))$ . For the control pure POPC symmetric bilayer, it is seen that the trajectories are purely diffusive ( $\langle \delta r_i(t)^2 \rangle \propto t$ ) in nature. For the ternary bilayer, however, this MSD would exhibit deviations from true diffusion, which can be characterized by  $\langle \delta r_i(t)^2 \rangle \propto t^\alpha$ . Figure 5c shows the MSD for the tagged lipids in both the symmetric and asymmetric bilayers and the corresponding values of the exponent  $\alpha$ . The value of  $\alpha$  obtained for SM in the asymmetric bilayer ( $\alpha \approx 0.39$ ) is consistent with the experimental value obtained by analyzing recent SPT of labeled SM on the plasma membrane of epithelial cells,  $\alpha \approx 0.3$ .<sup>33</sup> The interbilayer coupling in the symmetric ternary system, makes the tagged SM movement slower, as seen by the lower value of  $\alpha \approx 0.35$  (see Figure 5(c)). The tagged particle dynamics of the other lipids in the asymmetric bilayer, viz., POPC and cholesterol, show interesting differences between the two leaflets – typically, the upper leaflet lipids show a smaller  $\alpha$  ( $\alpha = 0.45, 0.41$ , respectively), than the lower leaflet lipids ( $\alpha = 0.85, 0.89$ , respectively).

## Conclusion

The cell membrane exhibits both lateral and transverse heterogeneity. In this paper, the equilibrium properties of a ternary component asymmetric bilayer membrane system at  $l_o$ - $l_d$  phase coexistence are studied using an atomistic MD simulation over a time scale of 220 ns. The asymmetric bilayer considered in this study is composed of POPC, SM and cholesterol in the ratio of 1:1:1 in the upper leaflet and POPC and cholesterol in the lower leaflet. The two significant results from this study are: (i) cholesterol prefers to be associated with SM-rich domains ( $l_o$ -like) three times more than POPC-rich domains ( $l_d$ -like) and (ii) the saturated lipid SM in the  $l_o$ -like domain exhibits long-range tilt correlations purely as a result of the asymmetry in the bilayer composition (in contrast,

the SM lipid molecules in the symmetric bilayer show no such tilt).

This bilayer-asymmetry induced lipid tilt in the  $l_o$ -like domain has important implications to local membrane deformation and hence membrane budding and endocytosis. The existence of a lipid tilt expressed over large scales provides a natural coupling to the local curvature tensor, and results in anisotropic bending stresses at the membrane.<sup>57</sup> Moreover, if the constituent lipids are chiral (as they are in ‘raft’-lipids), then there would be additional bending stresses serving to deform the membrane locally. When the strength of these couplings are large enough, they can induce the local formation of spherical buds or cylindrical tubules. Recent FRET-based studies of the organization of lipid tethered proteins on the outer surface of living cells, such as GPI-anchored proteins, have shown that they form cholesterol sensitive nanoclusters mediated by the activity of cortical actin.<sup>6,7</sup> These studies imply that there must exist a molecular linkage between the outer leaflet GPI-anchored proteins and cortical actin. The current study will form the basis for further investigations on possible transbilayer interactions between GPI-anchored proteins, SM and cholesterol, with specific saturated, long chain lipids at the inner leaflet that have potential interactions with actin or actin remodeling proteins.

## Acknowledgement

We are very grateful to M. Karttunen for generous advice and help on the use of the simulation packages without which this work would not have been possible. We thank R. Sowdhamini for the use of computer facilities, and S. Mayor and V. A. Raghunathan for a critical reading of the manuscript. MR acknowledges a grant from HFSP and CEFIPRA 3504-2.

## References

- (1) P. F. Devaux and R. Morris. 2004. Transmembrane asymmetry and lateral domains in biological membranes. *Traffic* 5 : 241-246.
- (2) K. Simons and E. Ikonen. 1997. Functional rafts in cell membranes. *Nature* 387 : 569-572.

- (3) D. Lingwood and K. Simons. 2010. Lipid rafts as a membrane-organizing principle. *Science* 327 : 46 - 50.
- (4) S. Mayor and M. Rao. 2004. Rafts : Scale-dependent, active lipid organization at the cell surface. *Traffic* 5 : 231-240.
- (5) J. F. Hancock. 2006. Lipid rafts : contentious only from simplistic standpoints. *Nat Rev Mol Cell Bio* 7 : 456-462.
- (6) P. Sharma, R. Varma, R.C. Sarasij, K. Gousset, Ira, G. Krishnamoorthy, M. Rao and S. Mayor. 2004. Nanoscale organization of multiple GPI-Anchored proteins in living cell membranes. *Cell* 166 : 577-589.
- (7) D. Goswami, K. Gowrishankar, S. Bilgrami, S. Ghosh, R. Raghupathy, R. Chadda, R. Vishwakarma, M. Rao and S. Mayor. 2008. Nanoclusters of GPI-Anchored proteins are formed by cortical actin-driven activity. *Cell* 135 : 1085-1097.
- (8) M.D. Collins and S.L. Keller. 2007. Tuning lipid mixtures to induce or suppress domain formation across leaflets of unsupported asymmetric bilayers. *Proc Natl Acad Sci USA* 105:124-128.
- (9) S. L. Veatch and S. L. Keller. 2002. Organization in lipid membranes with cholesterol. *Phys Rev Lett* 89 : 268101-268104.
- (10) S. L. Veatch and S. L. Keller. 2003. Separation of lipid phases in giant vesicles of ternary mixtures of phospholipids and cholesterol. *Biophys J* 85 : 3074-3083.
- (11) T. Baumgart, S. T. Hess and W. W. Webb. 2003. Imaging coexisting domains in biomembrane models coupling curvature and line tension. *Nature* 425 : 821-824.
- (12) P. S. Niemela, S. Ollila, M. T. Hyvonen, M. Karttunen and I. Vattulainen. 2007. Assessing the nature of lipid raft membranes. *Plos Comput Biol* 3 : 0304 - 0312.

- (13) S. Esteban-Martin, H. J. Risselada, J. Salgado and S. J. Marrink. 2009. Stability of asymmetric lipid bilayers assessed by molecular dynamics simulations. *J. Am. Chem. Soc.* 131 : 15194 - 15202.
- (14) A. A. Gurtovenko and I. Vattulainen. 2007. Lipid transmembrane asymmetry in intrinsic membrane potential: Two sides of the same coin. *J. Am. Chem. Soc.* 129 : 5358 - 5359.
- (15) A. A. Gurtovenko and I. Vattulainen. 2008. Membrane potential and electrostatics of phospholipid bilayers with asymmetric transmembrane distribution of anionic lipids. *J. Phys. Chem. B* 112 : 4629 - 4634.
- (16) M. Laradji and P.B. Sunil Kumar. 2006. Anomalously slow domain growth in fluid membranes with asymmetric transbilayer lipid distribution. *Phys Rev E* 73 : 040901.
- (17) A. J. Wagner, S. Loew and S. May. 2007. Influence of monolayer-monolayer coupling on the phase behavior of a fluid lipid bilayer. *Biophys J* 93 : 4268 - 4277.
- (18) P. L. Hansen, L. Miao and J. H. Ipsen. 1998. Fluid lipid bilayers : intermonolayer coupling and its thermodynamic manifestations. *Phys Rev E* 58 : 2311 - 2323.
- (19) E. J. Wallace, N. M. Hooper and P. D. Olmsted. 2005. The kinetics of phase separation in asymmetric membranes. *Biophys J* 88 : 4072 - 4083.
- (20) D. W. Allender and M. Schick. 2006. Phase separation in bilayer lipid membranes : effects on the inner leaf due to coupling to the outer leaf. *Biophys J* 91 : 2928 - 2935.
- (21) E. Egberts, S.J. Marrink, H. J. C. Berendsen. 1994. Molecular dynamics simulation of a phospholipid membrane. *Eur. Biophys. J* 22 : 423 - 436.
- (22) O. Berger, O. Edholm, and F. Jahnig. 1997. Molecular dynamics simulations of a fluid bilayer of dipalmitoylphosphatidylcholine at full hydration, constant pressure, and constant temperature. *Biophys. J* 72 : 2002 - 2013.

- (23) D. P. Tieleman, L. R. Forrest, M. S. P. Sansom, and H. J. C. Berendsen. 1998. Lipid Properties and the Orientation of Aromatic Residues in OmpF, Influenza M2, and Alamethicin Systems: Molecular Dynamics Simulations. *Biochemistry* 37 : 17554 - 17561.
- (24) M. Höltje, T. Forster, B. Brandt, T. Engels, W. von Rybinski, and H. D. Höltje. 2001. Molecular dynamics simulations of stratum corneum lipid models: fatty acids and cholesterol. *Biochim. Biophys. Acta* 1511 : 156 - 167.
- (25) P. Niemelä, M. T. Hyvönen, and I. Vattulainen. 2004. Structure and Dynamics of Sphingomyelin Bilayer: Insight Gained through Systematic Comparison to Phosphatidylcholine. *Biophys. J.* 87 : 2976 - 2989.
- (26) Z. Zhang, S. Y. Bhide and M. L. Berkowitz. 2007. Molecular dynamics simulations of bilayers containing mixtures of sphingomyelin with cholesterol and phosphatidylcholine with cholesterol. *J. Phys. Chem.* 111 : 12888 - 12897.
- (27) G. A. Khelashvili and H. L. Scott. 2004. Combined Monte Carlo and molecular dynamics simulation of hydrated 18:0 sphingomyelin-cholesterol lipid bilayers. *Journal of Chemical Physics* 120 : 9841 - 9847.
- (28) J. Aittoneimi, P. S. Niemelä, M. T. Hyvönen, M. Karttunen, and I. Vattulainen. 2007. Insight into the putative specific interactions between cholesterol. *Biophysical Journal* 92 : 1125 - 1137.
- (29) H. Ohvo-Rekila. 2002. Cholesterol interactions with phospholipids in membranes. *Progress in lipid research* 41 : 66 - 97.
- (30) T. Rog. 2006. Cholesterol-sphingomyelin interactions: A molecular dynamics study. *Biophysical Journal* 91 : 3756 - 3767.
- (31) S. Y. Bhide, Z. Zhang and M. L. Berkowitz. 2007. Molecular dynamics simulations of SOPS and sphingomyelin bilayers containing cholesterol. *Biophysical Journal* 92 : 1284-1295.



- (32) A. Kusumi, C. Nakada, K. Ritchie, K. Murase, K. Suzuki, H. Murakoshi, R. S. Kasai, J. Kondo and T. Fujiwara. 2005. Paradigm shift of the plasma membrane concept from the two-dimensional continuum fluid to the partitioned fluid: High-Speed Single-Molecule Tracking of Membrane Molecules. *Annu Rev Biophys Biomol Struct* 34 : 351 - 378.
- (33) S. J. Sahl, M. Leutenegger, M. Hilbert , S. W. Hell and C. Eggeling. 2010. Fast molecular tracking maps nanoscale dynamics of plasma membrane lipids. *Proc Natl Acad Sci USA* 107 : 6829 - 6834.
- (34) D. P. Tieleman and H. J. C. Berendsen. 1998. A molecular dynamics study of the pores formed by Escherichia coli OmpF porin in a fully hydrated palmitoylcholine bilayer. *Biophys J* 74 : 2786 - 2801.
- (35) H. J. C. Berendsen, J. P. M. Postma, W. F. van Gunsteren and J. Hermans. 1981. Interaction models for water in relation to protein hydration. *Intermolecular Forces* pp. 331 - 342.
- (36) L. Martinez, R. Andrade, E. G. Birgin and J. M. Martinez. 2009. PACKMOL : A package for building initial configurations for molecular dynamics simulations. *Comput Chem J* 30 : 2157 - 2164.
- (37) R. Koynova and M. Caffrey. 1998. Phases and phase transitions of the phosphatidylcholines. *Biochim Biophys Acta* 1376 : 91 - 145.
- (38) R. Koynova and M. Caffrey. 1995. Phases and phase transitions of the hydrated sphingolipids. *Biochim Biophys Acta* 1255 : 213 - 236.
- (39) R. F. M. de Almeida, A. Fedorov and M. Prieto. 2003. Sphingomyelin/ Phosphatidylcholine/ Cholesterol phase diagram : boundaries and composition of lipid rafts. *Biophys J* 85 : 2406 - 2416.
- (40) E. Lindahl, B. Hess and van der Spoel D. 2001. Gromacs 3.0 : A package for molecular simulation and trajectory analysis. *J Mol Mod* 7 : 306 - 317.

- (41) S. A. Safran. 1994. *Statistical Mechanics of Membranes and Interfaces* (Addison Wesley, Reading, Mass.).
- (42) M. Patra. 2005. Lateral pressure profiles in cholesterol-DPPC bilayers. *Eur Biophys J* 35 : 79 - 88.
- (43) A. J. Bray. 2002. Theory of phase-ordering kinetics. *Adv Phys* 51 : 481 - 587.
- (44) S. A. Pandit, E. Jakobsson, H. L. Scott. 2004. Simulation of the early stages of nano-domain formation in mixed bilayers of sphingomyelin, cholesterol and dioleoylphosphatidylcholine. *Biophysical Journal* 87: 3312 - 3322.
- (45) H. J. Risselada and S. J. Marrink. 2008. The molecular face of lipid rafts in model membranes. *Proc Natl Acad Sci USA* 105 : 17367 - 17372.
- (46) H. A. Riniaa, M. M. E. Snelb, J. P. J. M. van der Eerdenb and B. de Kruija. 2001. Visualizing detergent resistant domains in model membranes with atomic force microscopy. *FEBS Letters* 501 : 92 - 96.
- (47) P. M. Chaikin and T. C. Lubensky. 2000. *Principles of Condensed Matter Physics* (Cambridge University Press).
- (48) L. V. Schafer, D. H. de Jong, A. Holt, A. J. Rzepiela, A. H. de Vries, B. Poolman, J. A. Killian, and S. J. Marrink. 2011. Lipid packing drives the segregation of transmembrane helices into disordered lipid domains in model membranes. *Proc Natl Acad Sci USA* 108 : 1343 - 1348 .
- (49) H. A. Rinia, M. M. E. Snel, J. P. J. M. van der Eerden, B. de Kruijff. 2001. Visualizing detergent resistant domains in model membranes with atomic force microscopy. *FEBS Letters* 501 : 92 - 96.
- (50) S. P. Soni, D. S. LoCasio, Y. Liu, J. A. Williams, R. Bittman, W. Stillwell, and S. R. Wasall. 2008. Docosahexaenoic acid enhances segregation of lipids between raft and non-raft domains: 2H NMR study. *Biophysical Journal* 95 : 203 - 214.

- (51) A. J. García-Sáez, S. Chiantia and P. Schwille. 2007. Effect of Line Tension on the Lateral Organization of Lipid Membranes. *Journal of Biological Chemistry* 282 : 33537 - 33544.
- (52) D. A. Brown , and E. London. 2000. Structure and function of sphingolipid and cholesterol-rich membrane rafts. *J. Biol. Chem.* 275 : 17221 - 17224.
- (53) D. E. Saslowsky, J. Lawrence, X. Ren, D. A. Brown, R. M. Henderson, and J. M. Edwardson. 2002. Placental alkaline phosphatase is efficiently targeted to rafts in supported lipid bilayers. *J. Biol. Chem.* 277 : 26966 - 26970.
- (54) M. A. Kamal, A. Pal, V. A. Raghunathan and M. Rao. 2011. Theory of the asymmetric ripple phase in achiral lipid membranes. *EPL* 95 : 48004.
- (55) M. A. Kamal, A. Pal, V. A. Raghunathan and M. Rao. 2012. Phase behavior of two-component lipid membranes: theory and experiments. arXiv: 1203.5899v1 [cond-mat.soft].
- (56) E. B. Watkins, C. E. Miller, J. Majewski and T. L. Kuhl. 2011. Membrane texture induced by specific protein binding and receptor clustering: active roles for lipids in cellular function. *Proc Natl Acad Sci USA* 108 : 6975 - 6980.
- (57) R. C. Sarasij, S. Mayor and M. Rao. 2007. Chirality induced budding : a raft-mediated mechanism for endocytosis and morphology of caveolae ? *Biophys J* 92 : 3140 - 3158.
- (58) G. Lindblom, G. Orädd and A. Filippov. 2006. Lipid lateral diffusion in bilayers with phosphatidylcholine, sphingomyelin and cholesterol : An NMR study of dynamics and lateral phase separation. *Chem and Phys of Lipids* 141 : 179 - 184.
- (59) A. Pralle, P. Keller, E. L. Florin, K. Simons and J.K. Hörber. 2000. Sphingolipid-Cholesterol Rafts Diffuse as Small Entities in the Plasma Membrane of Mammalian Cells. *Cell Biol J* 148 : 997 - 1008.

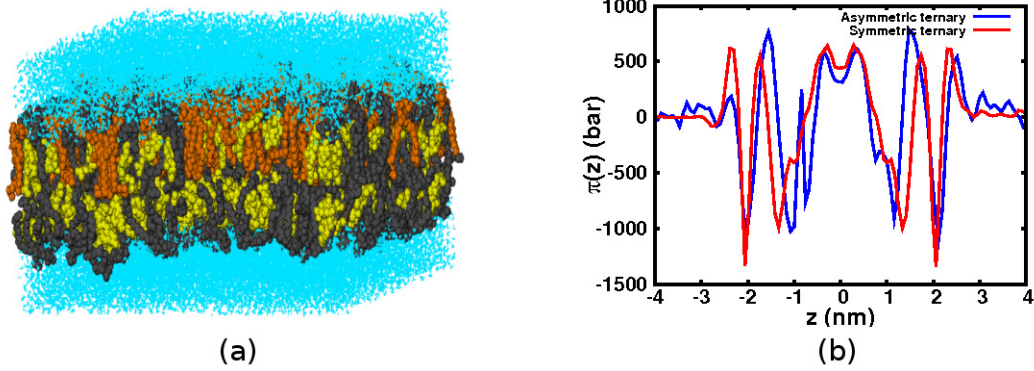


Figure 1: (a) Snapshot (side view) at the end of the simulation of the ternary system POPC (gray), SM (orange), Chol (yellow) forming the stable asymmetric bilayer in water (cyan). (b) Lateral pressure profiles  $\pi(z)$  as a function of position across the bilayer, for the ternary asymmetric bilayer (blue), and the ternary symmetric bilayer (red).

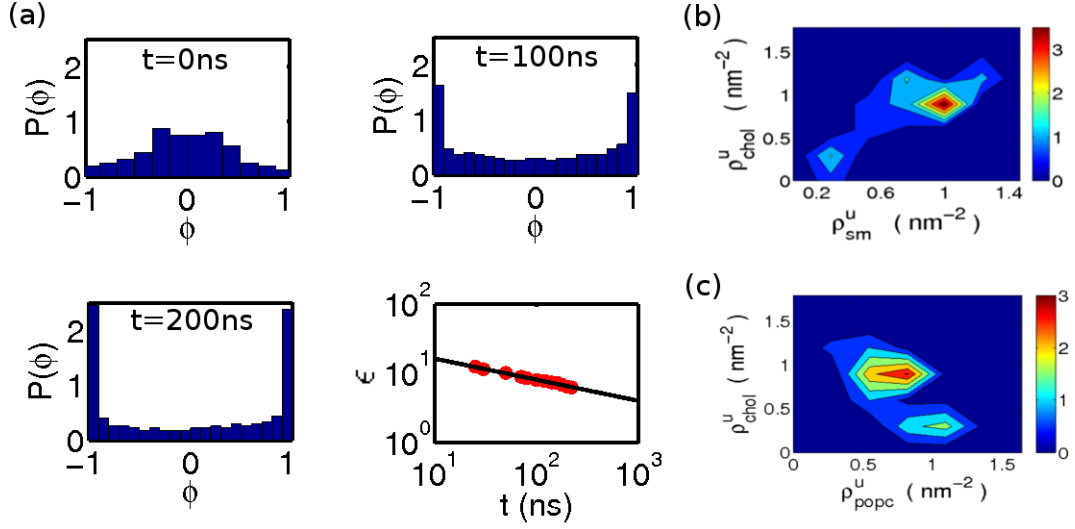


Figure 2: (a) Probability distribution  $P(\phi)$  (normalized) of the order parameter  $\phi = \frac{\rho_{\text{SM}} - \rho_{\text{POPC}}}{\rho_{\text{SM}} + \rho_{\text{POPC}}}$ , where  $\rho_{\text{SM}}$  and  $\rho_{\text{POPC}}$  are the concentrations of SM and POPC, respectively. Its time dependence from  $t = 0 - 200$  ns, shows that the system, initially prepared in the mixed state ( $\phi = 0$ ), has coarsened into SM rich ( $\phi = 1$ ) and POPC rich ( $\phi = -1$ ) domains separated by sharp interfaces. The last panel shows the dependence of the energy density  $\epsilon$  with time. The data (red filled circles) suggests that  $\epsilon$  goes as a power-law,  $\epsilon \sim t^{-3 \pm 0.15}$  (fitted line), with an exponent consistent with dynamical scaling,  $z = 3$  (see text). (b) Joint probability distribution (color bar) of the concentration (in units of number/ $\text{nm}^2$ ) of (b) SM and Chol and (c) POPC and Chol, coarse-grained over  $[1.73 \text{ nm}]^2$  in the upper leaflet and averaged over 20 ns. Red shows the highest joint probability and blue the lowest. Note the strong correlation (anticorrelation) between SM-Chol (POPC-Chol), respectively. The figures clearly show an enrichment of cholesterol in SM-enriched domains by a ratio 3 : 1

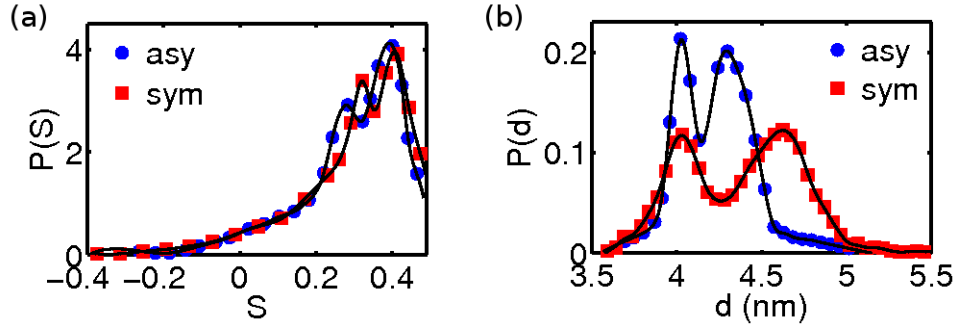


Figure 3: (a) Probability distribution of the deuterium order parameter  $S$  in the asymmetric (blue) and symmetric (red) bilayers. This is then coarse-grained over a spatial scale of 1.56 nm and time scale of 20 ns. Here  $S$  of the selected carbons (C5-C7) of POPC and SM is displayed, after suitable binning in the  $xy$ -plane. with the lower branch 0.1 – 0.26 corresponding to the low partitioning of SM in the  $l_d$  phase and the higher branch 0.35 – 0.45 corresponding to its enrichment in the  $l_o$  phase. (b) Probability distribution of the bilayer thickness  $d$  in the asymmetric (blue) and symmetric (red) bilayers. The two distinct peaks in the asymmetric bilayer at 4 nm and 4.3 nm indicates the coexistence of the  $l_d$  and  $l_o$  phases. The local bilayer thickness is constructed by via  $x$ - $y$  grids for the upper and lower leaflet of the bilayer, with grid size = 1.95 nm. An average over the  $z$ -coordinates of the phosphorus atom in the head groups of POPC and SM within each  $x$ - $y$  grid is then performed. The difference between the  $z$ -coordinates corresponding to the same  $x$ - $y$  grid of the two leaflets gives the local bilayer thickness.

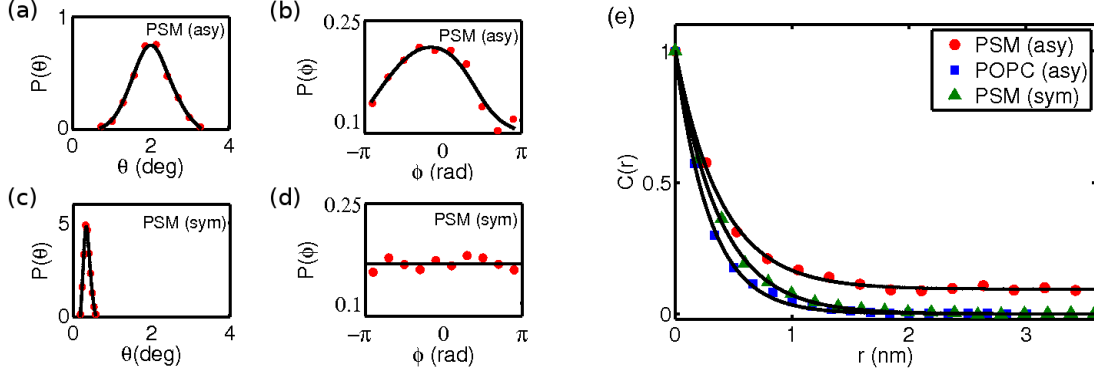


Figure 4: Probability distribution of the coarse-grained tilt angles  $\theta$  and  $\phi$  of SM (see text) in (a, b) the asymmetric bilayer, and (c, d) symmetric bilayer, respectively. These data are collected from equilibrium configurations that exhibit complete phase segregation, where the domain size is about half the system size. In the asymmetric ternary bilayer, SM exhibits a measurable tilt, as evidenced from the distributions of  $\theta$  and  $\phi$ . In comparison, SM in the symmetric bilayer shows an absence of tilt – the distribution of  $\theta$  is peaked at a value close to 0, while the distribution of  $\phi$  is uniform. (e) The tilt correlation function  $C(r) \equiv \langle \phi(r)\phi(0) \rangle$ , normalized to its value at  $r = 0$ , shows an exponential decay to zero for POPC (asymmetric bilayer) and SM (symmetric bilayer). However SM in the asymmetric bilayer shows an exponential decay to a *nonzero value*, demonstrating long range tilt correlations. The correlation length, defined by the scale at which  $C(r)$  decreases to  $1/e$  of its value at  $r = 0$ , can be easily read out,  $\xi_{SM}(sym) = 0.35 \text{ nm}$ ,  $\xi_{SM}(asy) = 0.5 \text{ nm}$  and  $\xi_{POPC}(asy) = 0.3 \text{ nm}$ .

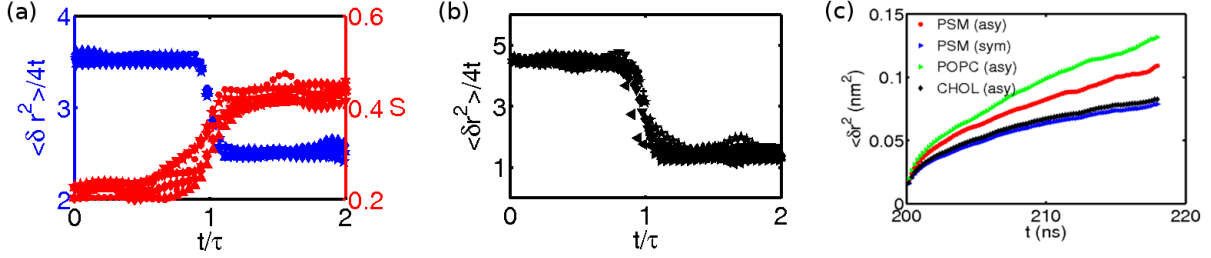


Figure 5: Mean square displacement of tagged particles as a function of time collected at high resolution over short time scales. Tagged particle diffusion of (a) SM and (b) Chol in the asymmetric bilayer—statistics collected over 6 tagged particles, each starting from the  $l_d$  domain, shows a data collapse onto a nonlinear crossover scaling curve. The crossover from high to low diffusion occurs at a time  $\tau$ , computed as the first-passage time of the tagged particle. For SM, we find that  $D_0 = 3.49\mu\text{m}^2\text{s}^{-1}$  and  $D_\infty = 2.69\mu\text{m}^2\text{s}^{-1}$ , while for Chol,  $D_0 = 4.23\mu\text{m}^2\text{s}^{-1}$  and  $D_\infty = 1.36\mu\text{m}^2\text{s}^{-1}$ . Note that in (a) as SM moves across domains, the deuterium order parameter  $S$  of tagged SM shows a similar crossover, going from  $\sim 0.22$  ( $l_d$ ) to  $\sim 0.42$  ( $l_o$ ). (c) MSD versus time with fits to  $\langle \delta r_i(t)^2 \rangle \propto t^\alpha$ , for SM in the asymmetric ( $\alpha = 0.39$ ) and symmetric bilayers ( $\alpha = 0.35$ ), and POPC and Chol in the upper leaflet of the asymmetric bilayer ( $\alpha = 0.45$  and  $0.41$ , respectively). Note that the  $\alpha$  exponent for SM in the symmetric bilayer is smaller than the asymmetric bilayer, due to the transbilayer coupling. Likewise, the MSD for POPC and Chol in the symmetric ternary bilayer are shown in Supplementary Figure S10, for comparison.



## Supplementary Information

A. Polley et al.

### Tabulation of force, torque and tension in model bilayers at equilibrium

#### 1. Components of Force

POPC (symmetric)

$$F_1 = 0.83 \pm 1.66 \text{ nN}, F_2 = 0.27 \pm 1.14 \text{ nN}, F_3 = -0.16 \pm 1.25 \text{ nN}$$

POPC-CHOL (symmetric)

$$F_1 = -1.01 \pm 1.36 \text{ nN}, F_2 = -0.32 \pm 2.72 \text{ nN}, F_3 = 0.18 \pm 0.62 \text{ nN}$$

#### 2. Components of the moment of force

POPC (symmetric)

$$M_{12} = 8.26 \pm 0.102 \text{ nN}\cdot\text{nm}, M_{13} = 10.74 \pm 0.066 \text{ nN}\cdot\text{nm}, M_{23} = 9.33 \pm 0.094 \text{ nN}\cdot\text{nm}$$

POPC-CHOL (symmetric)

$$M_{12} = 5.94 \pm 0.082 \text{ nN}\cdot\text{nm}, M_{13} = 8.882 \pm 0.23 \text{ nN}\cdot\text{nm}, M_{23} = 10.757 \pm 0.42 \text{ nN}\cdot\text{nm}$$

#### 3. Surface Tension

POPC (symmetric)

$$\gamma = 0.0204 \pm 0.0357 \text{ bar}\cdot\text{nm}$$

POPC-CHOL (symmetric)

$$\gamma = 0.0054 \pm 0.0099 \text{ bar}\cdot\text{nm}$$

The values of the components of force, moment of force and surface tension in these symmetric 1 and 2 component systems are comparable to those of the asymmetric ternary system given in the main text. This implies that the asymmetric ternary bilayer is as mechanically stable as the symmetric systems.

# Supplementary Figures

## A. Polley et al.

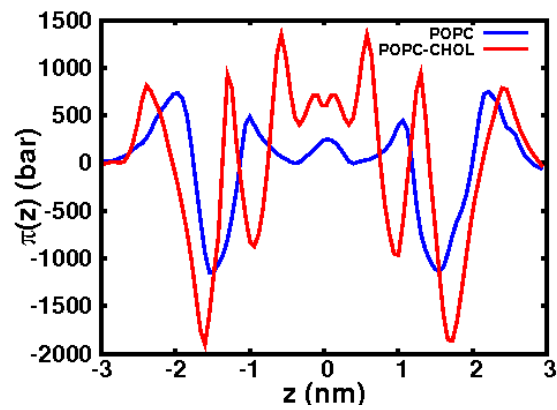


Figure 1: Lateral pressure profile of the symmetric bilayer made of (a) pure POPC (blue) and (b) POPC + Chol, with ratio 1 : 1 (red).

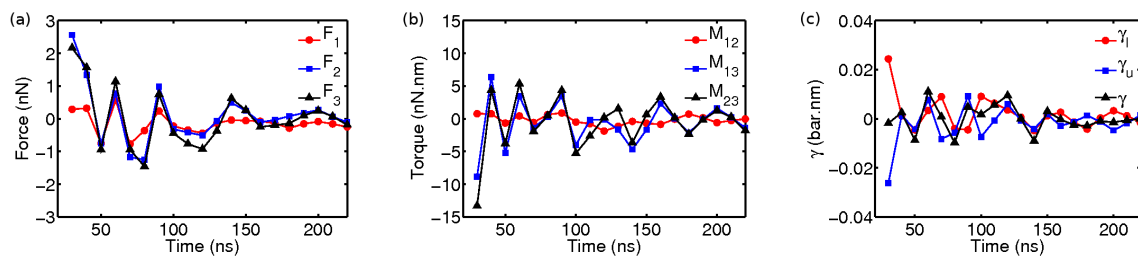


Figure 2: (a) Time dependence of the components of the force (defined in main text), where each data point is an average over 10 ns . (b) Time dependence of the components of the torque (defined in main text) where each data point is averaged over 10 ns. The observation that at late times these components fluctuate about zero, and that these fluctuations are not large, implies that in the mean there is force and torque balance. (c) The time dependence of the surface tension (evaluated from the components of the stress tensor) in the upper ( $\gamma_u$ ) and lower ( $\gamma_l$ ) leaflets of the membrane and the total surface tension ( $\gamma$ ). The observation that both  $\gamma_u$  and  $\gamma_l$  are small and fluctuate about zero, implies that in the mean there is no imbalance of surface tension in the two leaflets. The observation that the total  $\gamma$  is small and fluctuates about zero implies that in the mean the bilayer membrane is tensionless.

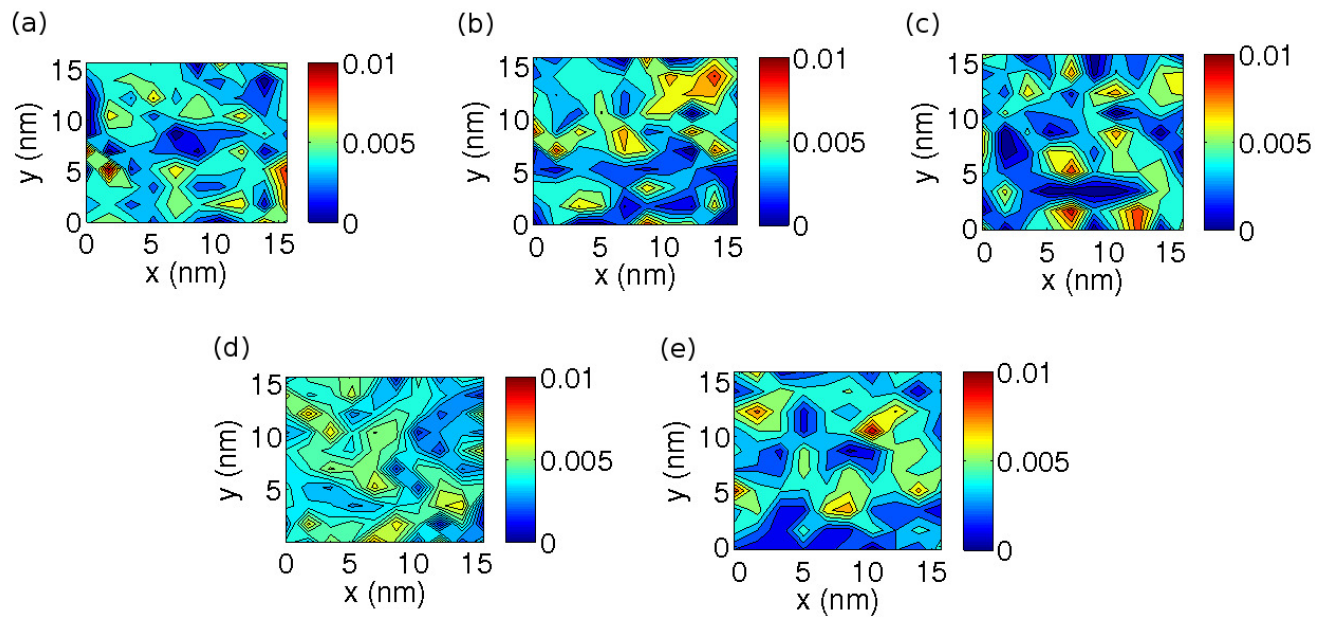


Figure 3: Spatial variation of lipid concentration in the asymmetric ternary bilayer system : (a) POPC, (b) PSM, (c) Chol in the upper leaflet, and (d) POPC and (e) Chol in the lower leaflet. The LUT bars denote the fraction of the lipid species within an area  $[1.56\text{nm}]^2$ .

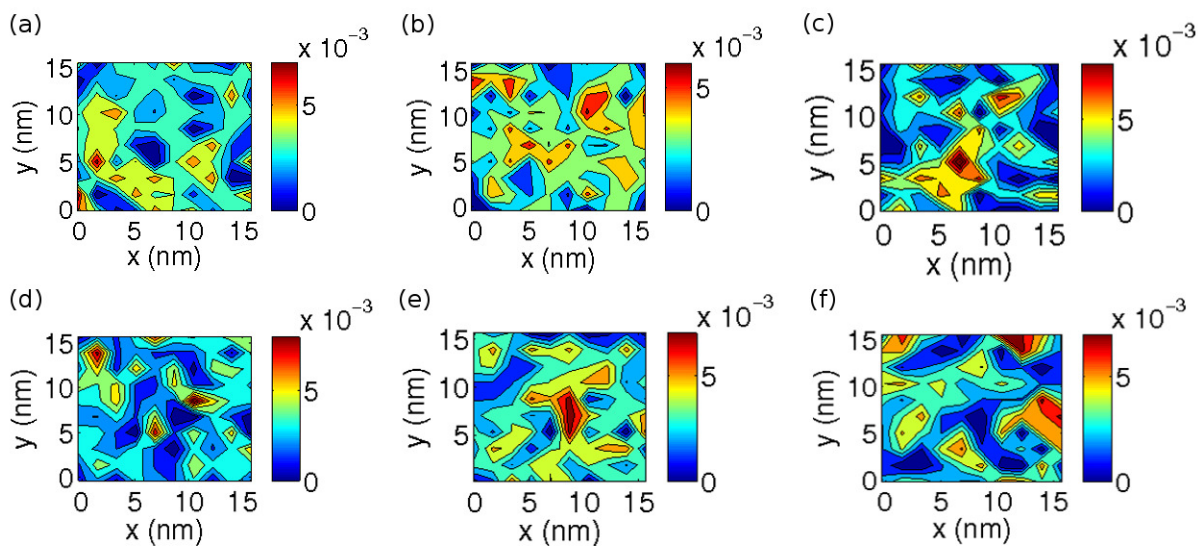


Figure 4: Spatial variation of lipid concentration in the symmetric ternary bilayer system : (a) POPC, (b) PSM, (c) Chol in the upper leaflet, and (d) POPC, (e) PSM and (f) Chol in the lower leaflet. The LUT bars denote the fraction of the lipid species within an area  $[1.56 \text{ nm}]^2$ . Note from (b) that the domain sizes are larger than in the asymmetric bilayer. Further, from (b) and (e), we note that there is significant registry of the domains across the bilayer (see Fig. 5).

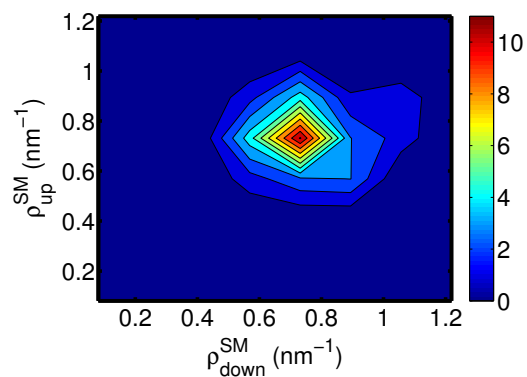


Figure 5: Joint probability distribution (color bar) of the concentration (in units of *number/nm*<sup>2</sup>) of SM of upper leaflet and SM at lower leaflet of symmetric ternary bilayer coarse-grained over  $[1.73 \text{ nm}]^2$  and averaged over 20 ns. Red shows the highest joint probability and blue the lowest. Note the strong correlation between SM-SM in the upper and lower leaflets implies significant bilayer registry in the SM-enriched domain across the two leaflets.

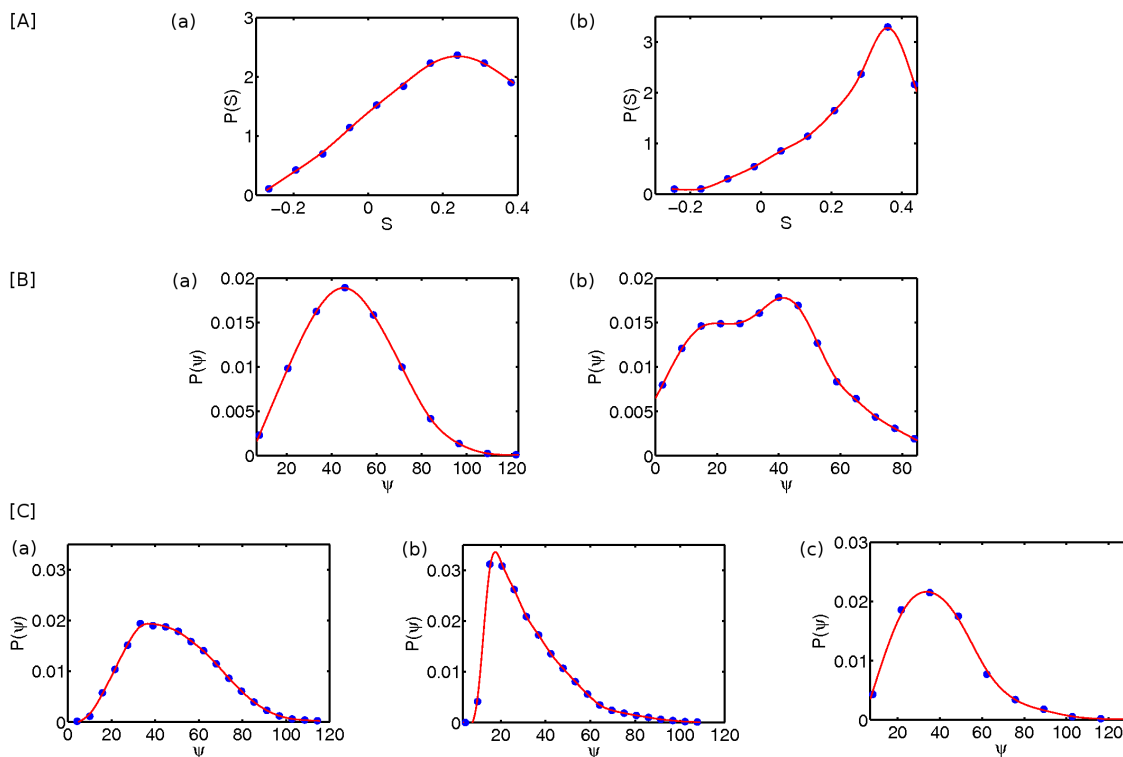


Figure 6: [A] Probability distribution of the deuterium order parameter  $S$  of POPC in the symmetric bilayer of (a) POPC and (b) POPC + CHOL (with ratio 1 : 1). [B] Probability distribution of splay of POPC in the symmetric bilayer of (a) POPC and (b) POPC-CHOL (with ratio 1 : 1). [C] Probability distribution of splay of (a) POPC and (b) PSM in the upper leaflet and (c) POPC in the lower leaflet of the asymmetric ternary bilayer.

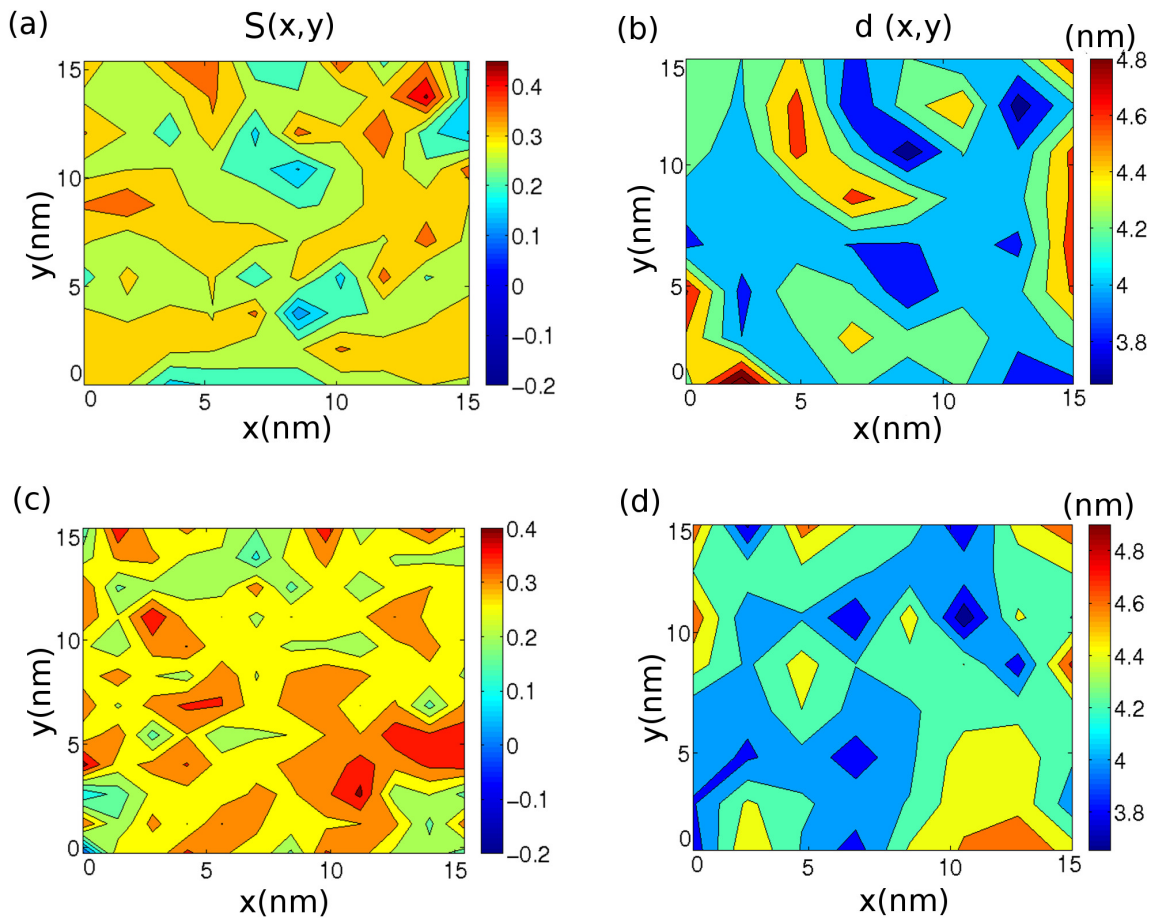


Figure 7: Spatial variation of deuterium order parameter  $S(x,y)$  and bilayer thickness  $d(x,y)$  of (a-b) asymmetric bilayer and (c-d) symmetric bilayer of the ternary system. In both cases, the domains coarsen over time; note however that the domain are larger in the symmetric bilayer compared to the asymmetric bilayer, evaluated over the same time. In addition, note that in the case of the symmetric bilayer, the domain registry across the bilayer is significant, consistent with Fig. 5.



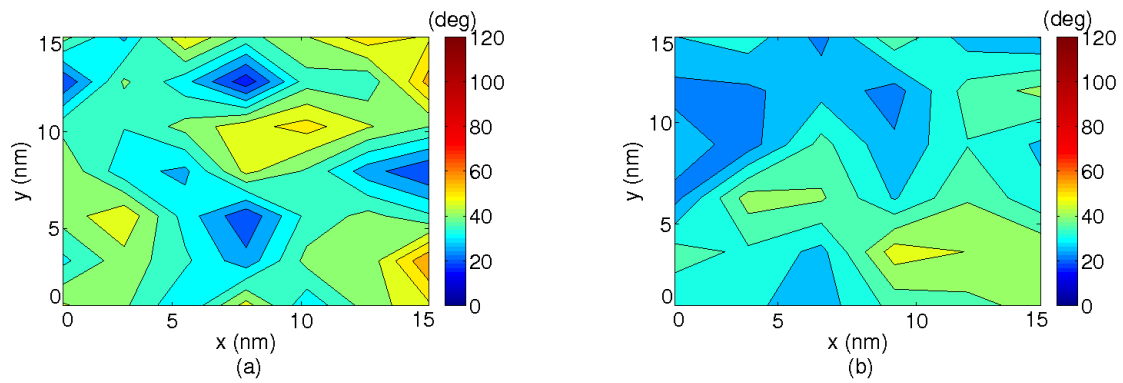


Figure 8: Spatial heterogeneity of splay of (a) POPC and (b) PSM in the upper leaflet of the asymmetric ternary bilayer.

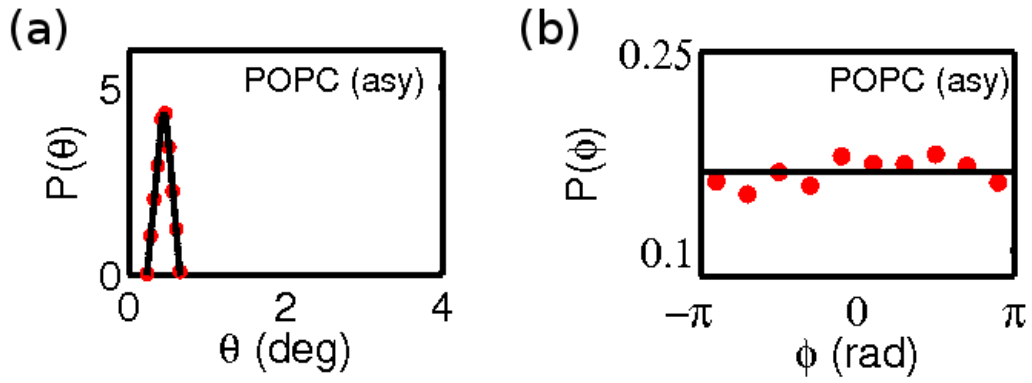


Figure 9: Probability distribution of the tilt angles (a)  $\theta$  and (b)  $\phi$  for POPC in the asymmetric ternary bilayer. Note that the distribution of  $\theta$  is peaked about  $\approx 0$ , while the distribution of  $\phi$  is uniform, consistent with the known fact that POPC does not exhibit a tilt at these temperatures.

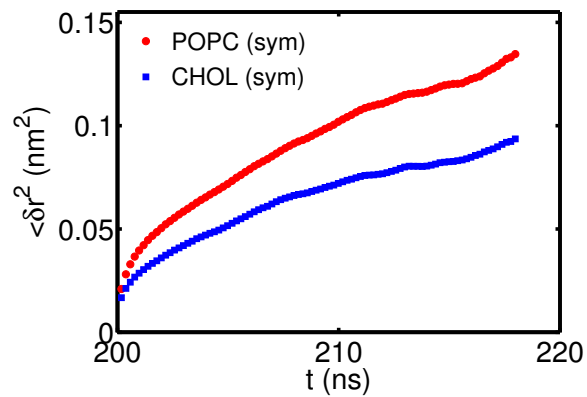


Figure 10: MSD versus time for tagged POPC and Chol in the symmetric ternary bilayer. Fits to  $\langle \delta r_i(t)^2 \rangle \propto t^\alpha$  gives  $\alpha = 0.35$  (POPC) and  $\alpha = 0.32$  (Chol). Note that the values of  $\alpha$  are consistently lower than those in the asymmetric ternary bilayer.